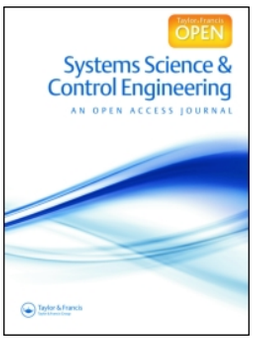

Systems Science & Control Engineering

An Open Access Journal

ISSN: (Print) 2164-2583 (Online) Journal homepage: http://www.tandfonline.com/loi/tssc20

Feedback control of oxygen uptake during robotics-assisted end-effector-based stair climbing

Jan Riedo & Kenneth J. Hunt

To cite this article: Jan Riedo & Kenneth J. Hunt (2017) Feedback control of oxygen uptake during robotics-assisted end-effector-based stair climbing, Systems Science & Control Engineering, 5:1, 142-155, DOI: 10.1080/21642583.2017.1297261

To link to this article: http://dx.doi.org/10.1080/21642583.2017.1297261

Published online: 12 Mar 2017.

SYSTEMS SCIENCE & CONTROL ENGINEERING: AN OPEN ACCESS JOURNAL, 2017
VOL. 5, 142–155
http://dx.doi.org/10.1080/21642583.2017.1297261

Taylor & Francis
Taylor & Francis Group

Feedback control of oxygen uptake during robotics-assisted end-effector-based stair climbing

Jan Riedo and Kenneth J. Hunt

Institute for Rehabilitation and Performance Technology, Division of Mechanical Engineering, Department of Engineering and Information Technology, Bern University of Applied Sciences, Burgdorf, Switzerland

ABSTRACT

A heart rate (HR) feedback control system for end-effector gait rehabilitation robots was previously developed and successfully tested, but oxygen uptake ($\dot{V}O_2$) is thought to better characterize physiological exercise intensity. The aim of the present study was to identify and compare $\dot{V}O_2$ and HR dynamics, and to develop and test a $\dot{V}O_2$ controller for an end-effector robot operated in stair climbing mode. Six able-bodied subjects were recruited for controller testing. Command response, disturbance rejection and robustness were assessed by means of three quantitative outcome measures: root-mean-square (RMS) error of $\dot{V}O_2$ ($RMSE_{\dot{V}O_2}$), average control signal power ($P_{\Delta P}$) and RMS error of volitionally controlled power ($RMSE_P$). The nominal first-order linear model for $\dot{V}O_2$ had time constant $\tau = 52.4$ s and steady-state gain $k = 0.0174$ (l/min)/W. The mean time constant $\tau = 67.3$ s for HR was significantly higher than for $\dot{V}O_2$, where $\tau = 53.4$ ($p = 0.048$). Command responses for a target $\dot{V}O_2$ profile gave consistent and accurate tracking with $RMSE_{\dot{V}O_2} = 0.198 \pm 0.070$ l/min, $P_{\Delta P} = 2.15 \pm 0.70\,W^2$ and $RMSE_P = 39.2 \pm 15.4$ W (mean ± SD). Disturbance rejection performance was also found to be satisfactory. The results of the controller tests confirm the feasibility of the proposed $\dot{V}O_2$ feedback control strategy. Robustness was verified as the single LTI controller was specific to only one of the subjects and no difference in outcome values was apparent across all subjects. Subject-specific variability in breath-by-breath respiratory noise is the main challenge in feedback control of $\dot{V}O_2$.

ARTICLE HISTORY
Received 5 December 2016
Accepted 16 February 2017

KEYWORDS
Feedback control; oxygen uptake; end-effector-based exercise; stair climbing; linear control; physiological control

1. Introduction

Stroke is the second-most-common cause of death and long-term disability worldwide (Donnan, Fisher, Macleod, & Davis, 2008). Every second stroke leads to total or partial loss of walking ability (Mozaffarian et al., 2014). Furthermore, aerobic exercise capacity, which is defined using peak oxygen uptake, is 50% lower 30 days post stroke compared to standard values of age-matched healthy adults (Kelly, Kilbreath, Davis, Zeman, & Raymond, 2003; MacKay-Lyons & Makrides, 2002). Evidence suggests that intensive task-specific rehabilitation in all phases after stroke has a positive influence on the rehabilitation outcome (Billinger et al., 2014; Veerbeek et al., 2014). Not only are physical improvements possible, there is also evidence that cognitive function can be enhanced by early rehabilitation, depending on the amount of training (El-Tamawy, Abd-Allah, Ahmed, Darwish, & Khalifa, 2014).

It has been shown that a large volume of task-specific training is important (French et al., 2007; Langhorne, Coupar, & Pollock, 2009). Since conventional therapy is limited by fatigue of the physiotherapists, robotics-assisted devices can improve the quality of rehabilitation. Several studies investigated the effects of robotics-assisted gait rehabilitation, concluding that it is more effective when conventional therapy is combined with robotics-assisted training due to the higher volume and intensity of training that can be applied (Chang & Kim, 2013; Hesse, Tomelleri, Bardeleben, Werner, & Waldner, 2012; Mehrholz & Pohl, 2012). Intensive task-specific training not only enhances physical and coordination skills, but also enhances plastic changes in neural circuits (Hornby et al., 2011). Even in non-impaired individuals who are trying to improve in a certain field of physical activity, the volume and intensity of training are the most important factors for success (Schmidt & Lee, 2011).

Due to the benefits of, and demand for, repetitive task-specific training, there is a steadily growing market for rehabilitation robots. Two main kinds of

CONTACT Jan Riedo jan.riedo@bfh.ch

gait rehabilitation robots can be identified: end-effector robots (Hesse, Waldner, & Tomelleri, 2010; Stoller, Schindelholz, Bichsel, & Hunt, 2014) and exoskeletons (Westlake & Patten, 2009). End-effector gait rehabilitation robots have an advantage concerning task-specific training because of the possibility to implement stair climbing activity (Hesse et al., 2010).

The studies reviewed above have focused on potential improvements in the ability to walk which can come about due to intensive, task-specific therapy and associated neurological adaptations. As a complement to this line of research, recent work has examined the applicability of gait-assistance robots for cardiovascular training and assessment. In this regard, several studies investigated the cardiopulmonary and cardiovascular responses to end-effector-based walking and stair climbing (Stoller et al., 2014; Stoller, Schindelholz, & Hunt, 2016), which confirmed that substantial increases in heart rate and respiration can be obtained from this form of exercise. A key observation was that response magnitudes are within the range required for positive training adaptations to take place within the cardiovascular system. A further breakthrough was made when the feasibility of implementing formal cardiopulmonary exercise testing (commonly referred to as CPET) in robotics-assisted end-effector-based stair climbing was confirmed (Stoller et al., 2016). From the perspective of control engineering applications, a novel and major advance was made when for the first-time automatic feedback principles were applied and successfully tested for control of heart rate and oxygen uptake on an exoskeleton system (Lokomat, Hocoma AG, Switzerland), (Schindelholz & Hunt, 2012, 2015).

A previous study, conducted using an end-effector gait rehabilitation robot (G-EO Evolution system, Reha Technology AG, Switzerland), implemented and tested a feedback system for control of heart rate (HR) (Riedo & Hunt, 2016). However, a more comprehensive physiological assessment consists of measurement of both heart rate and the rate of oxygen uptake (denoted $\dot{V}O_2$ and referred to in the sequel simply as 'oxygen uptake').

This observation provides the motivation for the problem investigated in the present work, namely the development of controllers for oxygen uptake. Oxygen uptake provides certain advantages over heart rate, as detailed below, but also presents additional difficulties. The principal difficulty lies in the more sophisticated sensor technology required to obtain oxygen uptake in real time, and also in the substantial breath-by-breath noise which affects this signal and which must be considered in the feedback design.

The principal advantage of using oxygen uptake rather than heart rate is that a more accurate determination of the physiological exercise intensity is possible. Exercise intensity is directly correlated with oxygen uptake and with cardiac output (rate of blood flow). Cardiac output is given by the product of heart rate and stroke volume (SV) but, for the sake of convenience, usually only the heart rate is measured. Since the autonomic nervous system continuously adjusts HR and SV to achieve a required cardiac output, the HR variable displays substantial lability. The problem of using HR to characterize exercise intensity is compounded by the fact that it is susceptible to external sensory influences such as noise, disturbances appearing in the visual field of the subject, or by other psychological factors.

Oxygen uptake, on the other hand, is given by the product of the volume of oxygen taken up per breath (cf. heart: stroke volume) and breathing frequency (cf. heart: heart rate). Direct measurement of $\dot{V}O_2$ therefore implicitly includes both of the subsidiary variables which are continuously adapted by the autonomic nervous system (namely uptake per breath and breathing frequency), and thus gives a stable and direct characterization of exercise intensity. This explains the observation that oxygen uptake is constant when training at a constant work rate but heart rate tends to continually increase over time: despite the increase in heart rate, cardiac output stays the same, presumably due to a downward autonomous regulation of stroke volume. It is therefore recommended to prescribe training intensity using oxygen uptake (Garber et al., 2011; Kenney, Wilmore, & Costill, 2015; Pescatello, Arena, Riebe, & Thompson, 2014).

The feedback structure employed here for control of oxygen uptake is based on a method previously proposed for HR control (Riedo & Hunt, 2016). The principal challenge for HR control was to deal appropriately with broad-spectrum heart rate variability, whereas for control of oxygen uptake it is the breath-by-breath variability of $\dot{V}O_2$ which is important. The purposely low-pass characteristics of the control approach developed in Riedo and Hunt (2016) therefore promised to be suitable for this new application also. A further contribution of the present work is a comparison of HR and $\dot{V}O_2$ dynamics, because HR can conveniently be measured simultaneously with $\dot{V}O_2$: based on previous studies using other exercise modalities (Bearden & Moffatt, 2001; Zhang et al., 2014), it was hypothesized that the time constant of the heart rate response would be higher than that for oxygen uptake.

The aim of this study was to identify and compare oxygen uptake and heart rate dynamics, and to develop and test an oxygen uptake controller for an end-effector gait rehabilitation robot using the stair climbing mode of operation.

2. Methods

2.1. Materials, overall identification and control structures

An end-effector gait rehabilitation robot was employed (G-EO Evolution system, Reha Technology AG, Switzerland; Figure 1). This provides three different trajectories: walking, stair climbing and stair descent. Stepping cadence and stepping height can be adjusted in the ranges 1–70 steps/min and 5–20 cm, respectively. The G-EO was augmented with a biofeedback-screen (Figure 1(B)), enabling the subject to perform volitional control of exercise work rate P (Figure 2(a)); the goal for the subject was to keep the actual value of P as close as possible to a target work rate P_{target}. P was calculated using the speed of the end-effectors (Figure 1(A)) and the forces applied on the footplates by the subject.

The volitional control structure with the human-in-the-loop work-rate controller was used for identification of $\dot{V}O_2$ and HR dynamics. For system identification, as far as HR and $\dot{V}O_2$ are concerned, this represents an open-loop structure wherein target work rate P_{target} was predefined as a series of steps (Figure 3(a)). For feedback control of $\dot{V}O_2$, the identification structure was then embedded within an outer automatic feedback control loop with the effective feedback controller transfer function $C(z^{-1}) = S(z^{-1})/R(z^{-1})$ (Figure 2(b)). The automatic controller continuously updated target work rate P_{target} on the basis of the measured actual oxygen uptake $\dot{V}O_2$ and a target/reference oxygen uptake profile $\dot{V}O_{2_{\text{target}}}$.

A breath-by-breath cardiorespiratory monitoring system (Metamax 3B, Cortex Biophysik GmbH, Germany) was used to measure $\dot{V}O_2$ in real time. Heart rate was measured with a chest belt (model T34, Polar Electro Oy, Finland) and a receiver (HRMI, Sparkfun Electronics, USA). With this system, individual breaths are analysed by means of gas sensors connected via a sampling line to the mask worn by the subject and a volume sensor embedded in the mask (Figure 1(C)). Real-time identification and feedback control systems used Labview (National Instruments Inc., USA), implemented directly on the computer embedded in the G-EO (Figure 1(D)). Offline data analysis and simulations were carried out using Matlab (MathWorks Inc., USA).

2.2. Plant model and system identification

For both oxygen uptake and heart rate dynamics identification, a first-order linear time-invariant (LTI) system was used, with parameters k, the steady-state gain, and τ, the time constant. Other studies have shown that this simple model can be sufficient for accurate feedback control of $\dot{V}O_2$ (Schindelholz & Hunt, 2015) as well as HR (Hunt & Fankhauser, 2016; Hunt, Fankhauser, & Saengsuwan, 2015; Riedo & Hunt, 2016). The model is expressed in continuous (P_c) and discrete (P_d) time as

$$u \to y : P_c(s) = \frac{k}{\tau s + 1} \overset{T_s}{\longleftrightarrow} P_d(z^{-1}) = \frac{B(z^{-1})}{A(z^{-1})} = \frac{b_0 z^{-1}}{1 + a_1 z^{-1}}. \quad (1)$$

Here, the double arrow denotes transformation between the continuous- and discrete-time domains with sample period T_s.

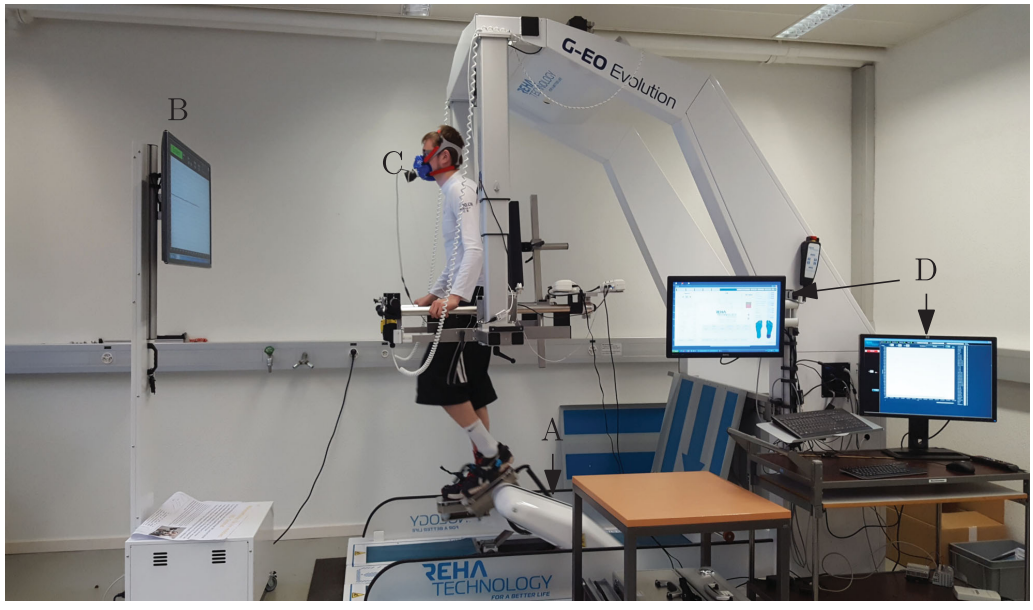

Figure 1. G-EO system with end-effectors (A) and biofeedback screen (B). Subject performing a test with a mask (C) for respiratory measurement. Operator screens (D) showing time courses of $\dot{V}O_2$, HR and P in real-time for monitoring.

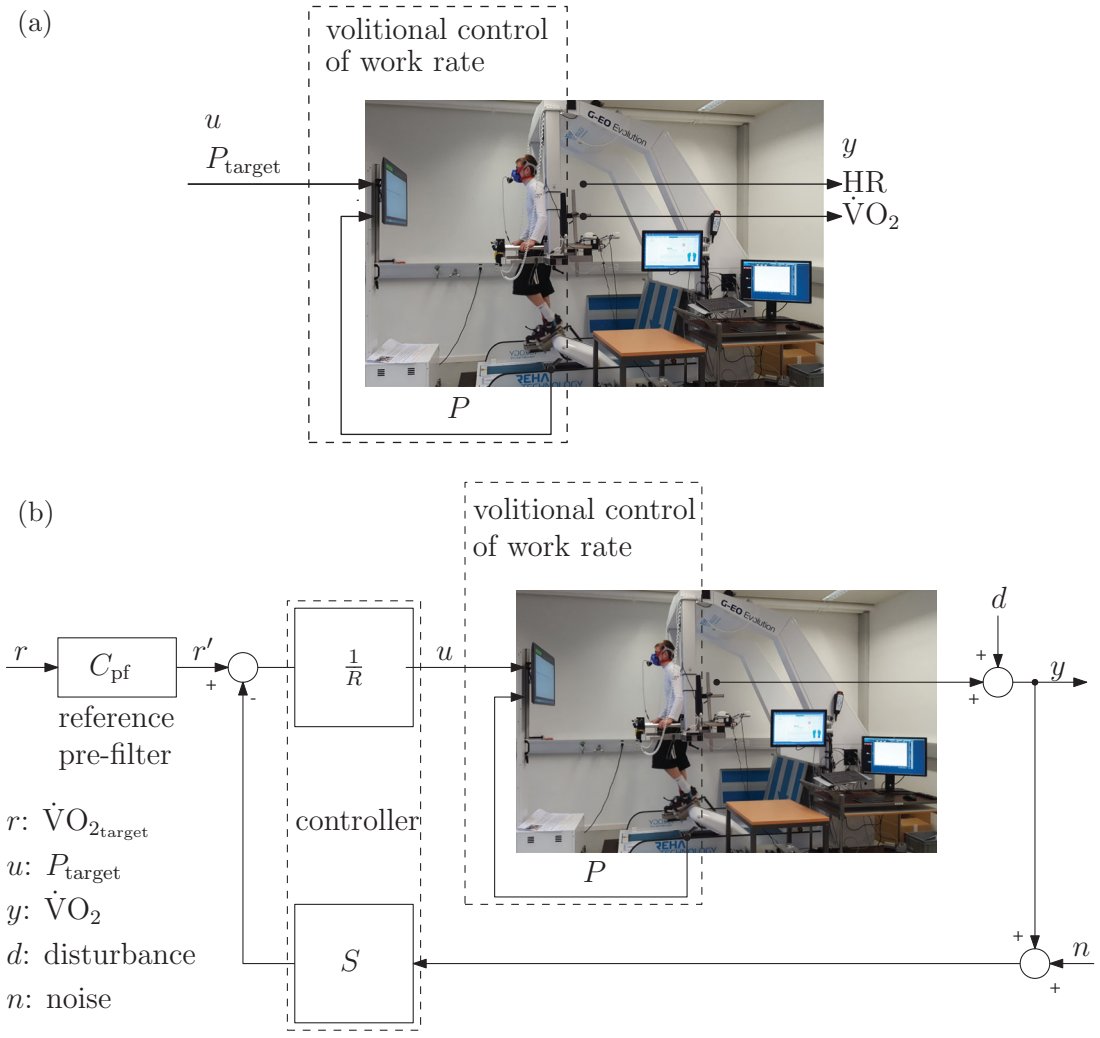

Figure 2. Structures for system identification and feedback control. (a) Open-loop structure for system identification. Within this structure, the subject performs volitional control of work rate. (b) Overall structure for closed-loop control of oxygen uptake. The controlled variable of the outer loop is the actual oxygen uptake $\dot{V}O_2$. The transfer function $u \rightarrow y$ from the target work rate P_{target} to actual oxygen uptake $\dot{V}O_2$ corresponds to Equation (1): $P_d(z^{-1})$, the plant model.

As shown in Figure 2(a), this model structure can be employed for the transfer functions from the target work rate P_{target} to $\dot{V}O_2$ and HR. These transfer functions thus include the inner volitional feedback control loop involving the subject as well as the physiological reaction of the subject.

Heart rate and oxygen uptake dynamics were both identified with a linear least-squares method on the basis of the first-order plant model in Equation (1). All six subjects (see Table 1) participated in the identification tests. Heart rate and oxygen uptake dynamics were identified using a single test for each subject. According to Figure 3(a), an individualized target work rate was defined with four changes, thus providing four step responses in HR and $\dot{V}O_2$. Identification was conducted within the time interval from 590 s to 1790 s in order to include all changes in target work rate but excluding start and end transients. Outcomes of the identification were the absolute root-mean-square model error (RMSE) and the normalized RMSE, which indicates the goodness of fit in percent (fit).

2.3. Controller design and analysis

For automatic feedback control of $\dot{V}O_2$, the structure in Figure 2(a) was supplemented with the outer closed loop shown in Figure 2(b). The measured plant output $\dot{V}O_2$ is fed back as a controller input, enabling the controller to continuously calculate P_{target} based on the control error between $\dot{V}O_{2_{target}}$ and $\dot{V}O_2$. The control design method developed in Riedo & Hunt (2016) for HR control was also applied here for control of $\dot{V}O_2$. This control approach applies three important constraints for the effective feedback controller transfer function $C(z^{-1}) = S(z^{-1})/R(z^{-1})$:

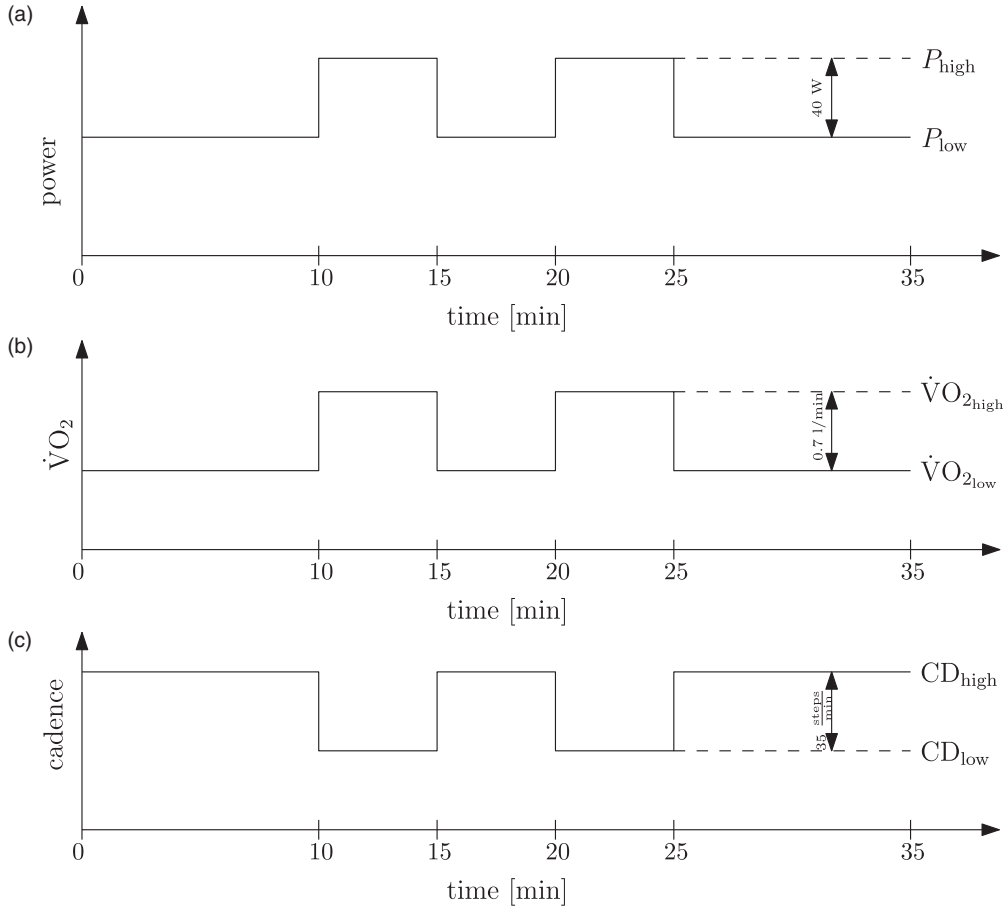

Figure 3. The step functions for identification, command response and disturbance rejection tests. (a) Time course of individually set target power P_{target} during identification sessions. Difference between P_{low} and P_{high} was 40 W for all subjects. The specific values can be found in Tables 2 and 3. (b) Time course of $\dot{V}O_{2_{target}}$ during command response tests. $\dot{V}O_{2_{high}}$ and $\dot{V}O_{2_{low}}$ were set individually for each subject. However, the difference between both levels was the same for all: $\dot{V}O_{2_{high}} - \dot{V}O_{2_{low}} = 0.7$ l/min. Numerical values are summarized in Table 4. (c) Time course of cadence (CD) during the disturbance rejection test. $\Delta CD = 35$ steps/min, $CD_{high} = 70$ steps/min and $CD_{low} = 35$ steps/min.

Table 1. Subject characteristics.

ID	Age (years)	Body mass (kg)	Height (cm)
S01	23	72	180
S02	24	87	183
S03	23	60	172
S04	26	83	183
S05	52	76	185
S06	25	89	182
mean ± SD	28.8 ± 11.4	78.2 ± 10.3	180.8 ± 4.6

Notes: ID: subject number; SD: standard deviation.

integrator (inclusion of $(1 - z^{-1})$ in $R(z^{-1})$), low-pass characteristics (inclusion of z^{-1} in $S(z^{-1})$, i.e. strictly causal) and a conservative pole cancellation strategy (inclusion of plant polynomial $A(z^{-1})$ in $S(z^{-1})$).

Full details of this feedback design method can be found in Riedo and Hunt (2016), and a brief summary is given here. Under the above constraints, the controller function C takes the form

$$C(z^{-1}) = \frac{S(z^{-1})}{R(z^{-1})} = \frac{z^{-1}(s_0 + s_1 z^{-1})}{(1 - z^{-1})R'(z^{-1})} = \frac{s_0 z^{-1} A(z^{-1})}{(1 - z^{-1})R'(z^{-1})} = \frac{s_0 z^{-1}(1 + a_1 z^{-1})}{(1 - z^{-1})(1 + r_1 z^{-1})}. \quad (2)$$

With the plant pole cancellation strategy, the characteristic polynomial of the feedback system is denoted $\Phi = A\Phi'$. The reduced polynomial Φ' is used in a pole assignment approach to define the behaviour of the controller. The coefficients ϕ_1 and ϕ_2 of Φ' are defined by specifying the nominal closed-loop rise time t_r and the damping factor ζ. Employing the above constraints, Φ' can be expressed in terms of the plant and controller

parameters as

$$\begin{aligned}\Phi'(z^{-1}) &= R + Bs_0z^{-1}\\ &= (1-z^{-1})(1+r_1z^{-1}) + b_0s_0z^{-2}\\ &= 1 + (r_1-1)z^{-1} + (b_0s_0 - r_1)z^{-2}\\ &= 1 + \phi_1z^{-1} + \phi_2z^{-2}.\end{aligned} \tag{3}$$

The algebraic solution for the controller parameters is then readily obtained by equating coefficients of like powers, giving

$$r_1 = \phi_1 + 1, s_0 = \frac{\phi_2 + r_1}{b_0} = \frac{\phi_1 + \phi_2 + 1}{b_0}. \tag{4}$$

A deterministic reference pre-filter C_{pf} was also employed in order to decouple the command signal from the feedback loop, as detailed in Riedo and Hunt (2016). This allows the definition of a separate rise time $t_{r_{\text{pf}}}$ and damping ζ_{pf} for the reference tracking response. C_{pf} is obtained from the overall pole polynomial Φ_{cl} for the reference response, which is in turn defined by the chosen $t_{r_{\text{pf}}}$ and ζ_{pf} values. This results in

$$C_{\text{pf}} = \frac{\Phi_{\text{cl}}(1)}{b_0} \cdot \frac{\Phi}{\Phi_{\text{cl}}}. \tag{5}$$

In order to perform a frequency–domain analysis of the influence of the disturbance d and the measurement noise n on the control signal u (see Figure 2(b)), the input sensitivity function U_o is employed, because U_o is the transfer function from the disturbance input to the control signal ($d \to u$) as well as from the noise input to the control signal ($n \to u$). The input sensitivity function U_o is defined as

$$\begin{aligned}d, n \to u : U_o &= \frac{C(z^{-1})}{1 + C(z^{-1})P_d(z^{-1})} = \frac{AS}{AR + BS}\\ &= \frac{AS}{\Phi} = \frac{S}{\Phi'}.\end{aligned} \tag{6}$$

Because of the constraint that the controller transfer function C has low-pass characteristics, it follows from the above equations that the input sensitivity function must be low-pass as well. Further reasoning for this can be found in Riedo and Hunt (2016). This feature is important as it ensures the control signal will not be excited by high-frequency components of the disturbance and measurement noise signals.

2.4. Data processing, outcome measures and analysis

Due to substantial breath-by-breath noise on the measured $\dot{V}O_2$ signal, which is typical for respiratory data, real-time data processing is essential. Three aspects were considered when designing a filtering strategy:

- Due to the real-time feedback control of $\dot{V}O_2$, the use of a moving average filter with zero phase shift was not possible. Thus, the more values that are averaged, the greater is the phase lag, resulting in a delayed reaction of the controller.
- There is no universal standard for data processing concerning breath-by-breath respiratory data. The most common procedure is either time averaging over a period of 15–30 s or a moving average of a certain number of breaths (e.g. 11 breaths as in Robergs, Dwyer, & Astorino, 2010). There is no recommendation specifically for real-time application as in feedback control of oxygen uptake.
- A factor of about 10 is recommended between averaging time and the system time constant (Åström & Wittenmark, 2011). The identification of $\dot{V}O_2$ in Section 3.1 revealed a mean time constant of $\tau = 48.3$ s thus the averaging time should be around 5 s.

In line with these considerations, a moving average of 4 breaths resulting in an averaging time of roughly 5 s (this is dependent on the changing breathing frequency) was implemented in real time for the variable $\dot{V}O_2$.

Three outcome measures serve as the basis for quantitative evaluation of controller performance, allowing comparison between the subjects and with other studies. RMS error for oxygen uptake tracking $\text{RMSE}_{\dot{V}O_2}$, average power of changes in target work rate $P_{\Delta P}$, and RMS tracking error of power RMSE_P were calculated as follows:

$$\text{RMSE}_{\dot{V}O_2} = \sqrt{\frac{1}{N}\sum_{i=1}^{N}(\dot{V}O_{2_{\text{sim}}}(i) - \dot{V}O_2(i))^2}. \tag{7}$$

Here, $\dot{V}O_{2_{\text{sim}}}(i)$ is obtained from simulation of the nominal closed-loop system, using the nominal plant model from Equation (1) and the calculated controller parameters.

$$P_{\Delta P} = \frac{1}{N-1}\sum_{i=2}^{N}(P_{\text{target}}(i) - P_{\text{target}}(i-1))^2. \tag{8}$$

The average power of the control signal $P_{\Delta P}$ gives a quantitative indication of the intensity of the control signal.

$$\text{RMSE}_P = \sqrt{\frac{1}{N}\sum_{i=1}^{N}(P_{\text{target}}(i) - P(i))^2}. \tag{9}$$

This value indicates how accurately a subject was able to follow the target work rate.

All three outcome values were calculated over a time period of 20 min, starting at 5 min to exclude the start-up transient. This time interval thus includes 5 min before the first change in target work rate as well as 5 min after the last change in target work rate.

2.5. Test protocol and subjects

All test profiles were individually tailored for each subject in order to apply an appropriate mean level of exercise intensity in each case, but the amplitude of steps in P_{target} (open-loop identification) and $\dot{V}O_{2_{target}}$ (closed-loop control) were kept the same for all subjects. All subjects took part in an identification and a control (command response) session. These tests were all conducted with a stepping cadence of 70 steps/min and a stepping height of 18 cm. Additionally, one subject participated in a disturbance rejection test (cadence was repeatedly changed as noted below), and another in a command response test with a non-low-pass controller. Each test was carried out on a different day.

Using data recorded in a previous study (Riedo & Hunt, 2016), appropriate work rate levels for each subject were determined for the identification tests. These measurements were conducted at moderate to vigorous intensity as predicted by heart rate and each subject's age. The mean value of P_{target} was subjected to a square-wave signal with an amplitude of 20 W (see Figure 3(a)).

To determine appropriate individual mean $\dot{V}O_2$ levels for the feedback control tests, the mean value of $\dot{V}O_2$ during identification sessions within the identification interval (590–1790 s) was calculated for each subject. This value was then employed as the mean value of $\dot{V}O_{2_{target}}$ for the command response tests. The amplitude of the $\dot{V}O_{2_{target}}$ square wave was calculated based on the intention to have approximately the same 20 W amplitude of target power during the command response tests as in the identification tests.

This was calculated based on the steady-state gain of the nominal model in Section 3.2, i.e. $k = 0.0174$ (l/min)/W. Thus,

$$\begin{aligned}\dot{V}O_{2_{target}} \pm \Delta\dot{V}O_2 &= \text{mean}(\dot{V}O_{2_{ident}}) \pm k \times 20\,\text{W} \\ &= \text{mean}(\dot{V}O_{2_{ident}}) \pm 0.35\,\text{l/min}. \quad (10)\end{aligned}$$

In order to test the disturbance rejection properties of the controller, a separate test with constant $\dot{V}O_{2_{target}}$ at the mean identification oxygen uptake level was conducted. A major disturbance was induced changing cadence stepwise between 70 and 35 steps/min. The downward change initially causes a reduction in velocity, therefore, the subject needs to increase the forces applied to the footplates in order to maintain the target power. Due to this increased effort, a higher oxygen uptake follows. The expectation is then that the controller will reduce target power with the result that $\dot{V}O_2$ should return to the target value. For changes from 35 back up to 70 steps/min, the converse response would be expected.

Six healthy males participated in this study (Table 1). No subject had any history of cardiovascular, pulmonary or musculoskeletal problems or current limitations in their physical ability. The study was reviewed and approved by the ethics committee of the Canton of Bern in Switzerland and all subjects provided written informed consent.

3. Results

3.1. Identification

The identified values for oxygen uptake dynamics were: steady-state gain $k = 0.0186 \pm 0.0029$ (l/min)/W (mean $\pm$ SD) and time constant $\tau = 53.4 \pm 4.1$ s. The overall fit was $62.5 \pm 12.6\%$ and RMSE was 0.12 ± 0.05 (l/min)/W. For the heart rate dynamics, the following values were identified: steady-state gain $k = 0.532 \pm 0.132$ bpm/W and time constant $\tau = 67.3 \pm 15.2$ s with overall fit $62.7 \pm 3.6\%$ and RMSE 3.27 ± 0.74 bpm/W. Individual values for steady-state gain k and time constant τ are summarized in Tables 2 and 3. Subject S02 had to be excluded from this analysis due to measurement error leading to a high level of breath-by-breath noise in $\dot{V}O_2$.

Exemplary plots of raw identification data are shown in Figure 4(a, c), and the corresponding model validation results in Figure 4(b, d). The identification interval (range of the x-axis in Figure 4(b, d)) is displayed using red bars in Figure 4(a, c) (590–1790 s). This includes 10 s before the first change in P_{target} and lasts for 20 min, including all changes in P_{target}.

All data sets for both $\dot{V}O_2$ and HR were used for the comparative analysis (Section 3.2). Furthermore, the identification results for $\dot{V}O_2$ dynamics were used to select a nominal model for $\dot{V}O_2$ controller calculation (Section 3.2).

3.2. Comparison of time constants and nominal model selection

The hypothesis that the time constant of heart rate dynamics is significantly higher than that of oxygen uptake was confirmed. Individual identified values of τ for $\dot{V}O_2$ and HR are plotted in Figure 5 (see also Tables 2 and 3). The mean values of τ for $\dot{V}O_2$ and HR were 53.4 ± 4.1 s and 67.3 ± 15.2 s, respectively. A single-sided t-test showed this difference to be significant with a p-value of 0.048 (the data were tested for a normal distribution with

Table 2. Results of oxygen uptake dynamics identification.

ID	P_{low} (W)	P_{high} (W)	k ($\frac{l/min}{W}$)	τ (s)	fit (%)	RMSE ($\frac{l/min}{W}$)
S01	60	100	0.0184	56.6	44.9	0.19
S03	70	110	0.0148	53.4	68.6	0.08
S04	90	130	0.0196	57.3	59.4	0.14
S05	30	70	0.0227	47.1	78.9	0.08
S06	70	110	0.0174	52.4	60.6	0.12
mean ± SD	64.0 ± 21.9	104.0 ± 21.9	0.0186 ± 0.0029	53.4 ± 4.1	62.5 ± 12.6	0.12 ± 0.05

Notes: ID: subject number; SD: standard deviation; P_{low}: individually chosen target power at low level; P_{high}: individually chosen target power at high level; k: steady-state gain of $\dot{V}O_2$ dynamics; τ: time constant of $\dot{V}O_2$ dynamics; fit: normalized RMSE of identified $\dot{V}O_2$ model and RMSE: root-mean-square error of $\dot{V}O_2$ model.

Table 3. Results of heart rate dynamics identification.

ID	P_{low} (W)	P_{high} (W)	k(bpm/W)	τ (s)	fit (%)	RMSE (bpm/W)
S01	60	100	0.704	75.1	69.0	3.43
S03	70	110	0.416	88.2	59.6	2.56
S04	90	130	0.428	55.2	61.9	2.87
S05	30	70	0.641	50.5	61.3	4.47
S06	70	110	0.470	67.8	61.8	3.04
mean ± SD	64.0 ± 21.9	104.0 ± 21.9	0.532 ± 0.132	67.3 ± 15.2	62.7 ± 3.6	3.27 ± 0.74

Notes: ID: subject number; SD: standard deviation; P_{low}: individually chosen target power at low level; P_{high}: individually chosen target power at high level; k: steady-state gain of HR dynamics; τ: time constant of HR dynamics; fit: normalized RMSE of identified HR model and RMSE: root-mean-square error of HR model.

the Lilliefors test). The mean difference was 14.0 s with a 95% confidence interval from 0.24 to ∞; the fact that the value 0 lies outwith this interval reflects the observed difference at the significance level of 5%. All values listed in Tables 2 and 3 were used for comparison, Subject S02 having been excluded as noted above.

In order to investigate the robustness of the overall $\dot{V}O_2$ control strategy, a single LTI model was selected as the nominal model for controller calculation. For this purpose, one of the individually identified models was selected as nominal, rather than using an average over several models/subjects. With this strategy, controller robustness can be better verified because potential differences between the identification subject and the other subjects can be analysed. The model selection procedure is visualized in Figure 5. Subject S05 was excluded from further consideration for the nominal model because of a distinctly higher value for steady-state gain k. It can be seen that the model for Subject S06 was closest to the average model of Subjects S01, S03, S04 and S06. Thus, the identified model for Subject S06 was selected as the nominal model and used for controller calculation. The nominal steady-state gain was therefore $k = 0.0174$ (l/min)/W and the nominal time constant was $\tau = 52.4$ s. A sampling period of $T_s = 5$ s was employed according to recommendations in Åström & Wittenmark (2011), Hunt & Hunt (2016) and Hunt & Fankhauser (2016). These choices give the nominal discrete-time model, Equation (1),

$$P_d(z^{-1}) = \frac{B(z^{-1})}{A(z^{-1})} = \frac{0.0016z^{-1}}{1 - 0.9090z^{-1}}. \quad (11)$$

3.3. Controller calculation

A single LTI controller was calculated according to Section 2.3 using the nominal model. The specifications used were: rise time $t_r = 195$ s, critical damping $\zeta = 1$ and sample period $T_s = 5$ s. This gave the controller Equation (2) as

$$C(z^{-1}) = \frac{S(z^{-1})}{R(z^{-1})} = \frac{z^{-1}(4.2785 - 3.8891z^{-1})}{(1 - z^{-1})(1 - 0.8354z^{-1})}. \quad (12)$$

The rise time of the reference pre-filter was set to $t_{r_{pf}} = 150$ s with the aim of having a relatively dynamic $\dot{V}O_2$ command response, when compared to the slower specification for the feedback loop. With $\zeta_{pf} = 1$, Equation (5) was used to obtain

$$C_{pf}(z^{-1}) = \frac{(7.0496827 - 19.3469229z^{-1} + 17.6981804z^{-2} - 5.3965933z^{-3})}{1 - 1.7886846z^{-1} + 0.7998482z^{-2}}. \quad (13)$$

With feedback controller Equation (12), the input sensitivity function U_o, Equation (6), has the desired low-pass characteristics (Figure 6, red line). The input sensitivity function for a controller with non-low-pass characteristics (used for comparative tests) is also plotted (Figure 6, blue line).

3.4. Controller tests

The quantitative outcome measures for all command response tests are summarized in Table 4 and the corresponding plots are shown in Figure 7. As with the identification tests, Subject S02 was excluded from the analysis due to excessive noise on the $\dot{V}O_2$ signal, which appears

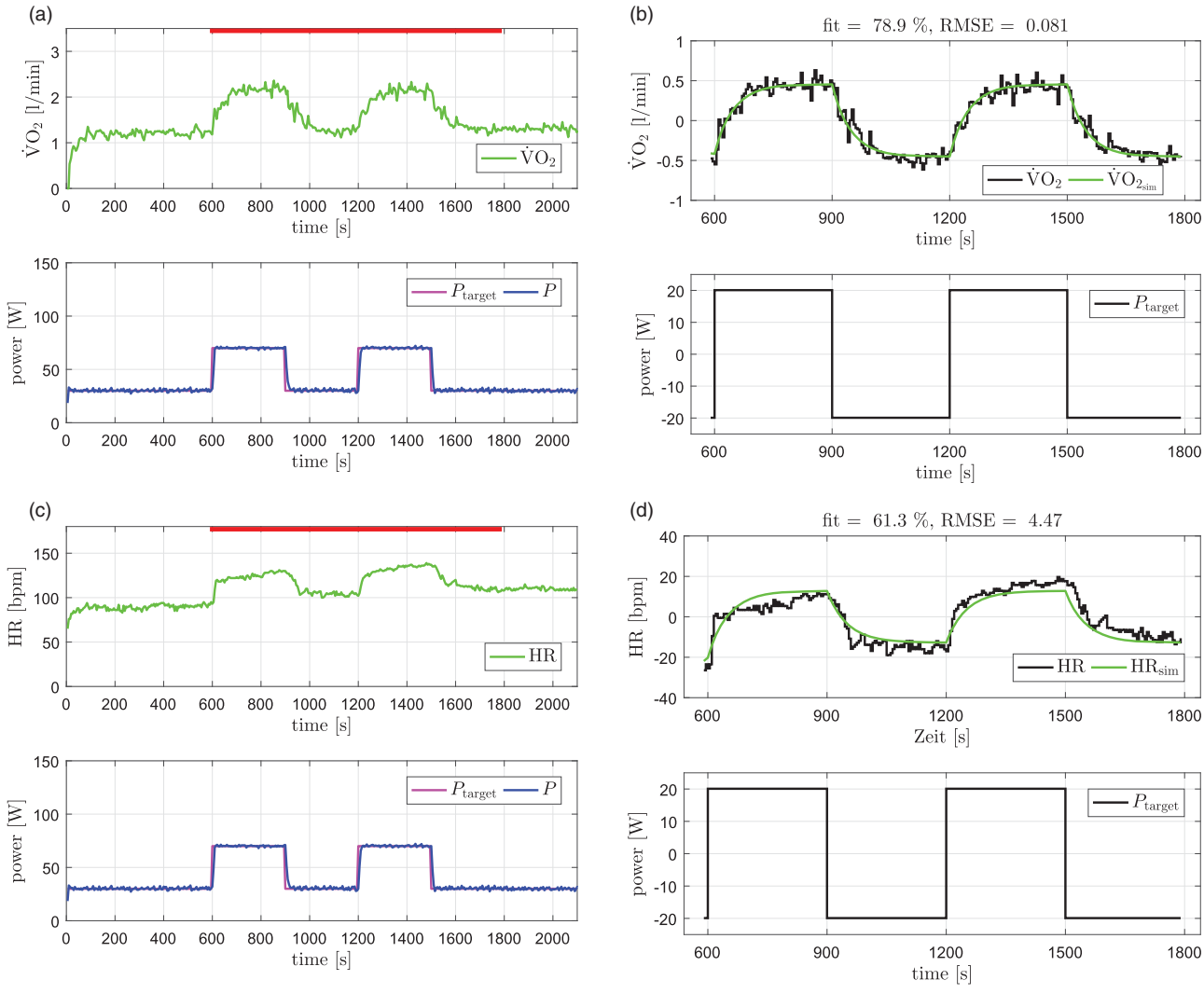

Figure 4. Exemplary plots of raw identification data (left column) and the corresponding model validation results (right column) of Subject S05. (a) Oxygen uptake: raw identification data, (b) model validation for oxygen uptake, (c) heart rate: raw identification data and (d) model validation for heart rate.

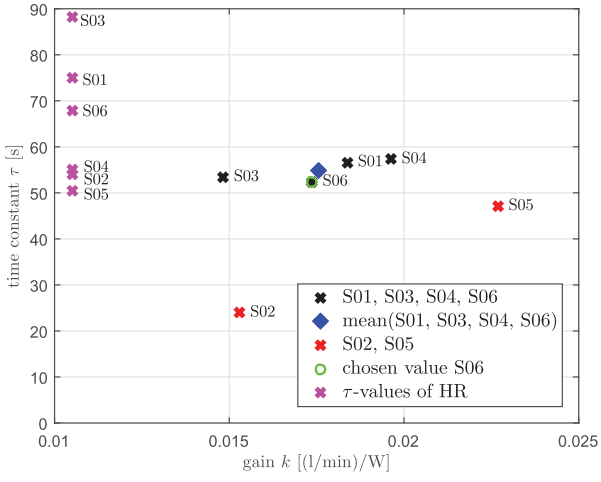

Figure 5. Plot of k and τ from oxygen uptake identification and, for comparison, τ for heart rate identification.

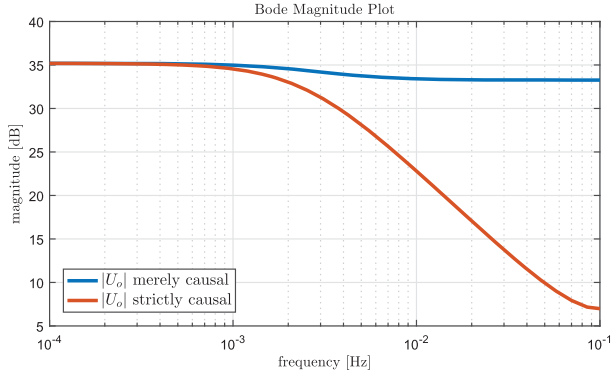

Figure 6. Bode magnitude plot of the input sensitivity function U_o with low-pass characteristics (red line), resulting from the strictly causal controller, and U_o based on a merely causal controller (blue line).

Table 4. Outcomes of the command response test.

ID	$\dot{V}O_{2_{mid}}$ (l/min)	$\dot{V}O_{2_{low}}$ (l/min)	$\dot{V}O_{2_{high}}$ (l/min)	$RMSE_{\dot{V}O_2}$ (l/min)	$P_{\Delta P}$ (W^2)	$RMSE_P$ (W)
S01	2.01	1.66	2.36	0.200	2.15	38.1
S03	2.08	1.74	2.43	0.135	1.64	29.0
S04	2.89	2.54	3.24	0.313	3.34	64.2
S05	1.73	1.38	2.08	0.148	1.66	24.6
S06	2.52	2.17	2.87	0.192	1.97	40.0
mean ± SD	2.25 ± 0.46	1.90 ± 0.46	2.60 ± 0.46	0.198 ± 0.070	2.15 ± 0.70	39.2 ± 15.3

Notes: ID: subject number; SD: standard deviation; $\dot{V}O_{2_{mid}}$: mid-level oxygen uptake (see Section 2.5); $\dot{V}O_{2_{low}}$: low-level oxygen uptake; $\dot{V}O_{2_{high}}$: high-level oxygen uptake; $RMSE_{\dot{V}O_2}$: RMS error of oxygen uptake; $P_{\Delta P}$: average power of the control signal; $RMSE_P$: root-mean-square error of volitionally controlled power.

to be a peculiarity of this particular subject's respiration rather than a property of the controller. The results otherwise demonstrate accurate and robust performance of the single LTI controller across all subjects.

Target oxygen uptake was tracked well in all cases with low $RMSE_{\dot{V}O_2}$ and the dynamic response of $\dot{V}O_2$ to changes in the target value was close to the nominal/simulated response. The control signal (P_{target}) was smooth in all cases, enabling the subjects to accurately follow P_{target} with low $RMSE_P$. Specifically, taken across all subjects, the performance outcomes were $RMSE_{\dot{V}O_2} = 0.198 \pm 0.070$ l/min, $P_{\Delta P} = 2.15 \pm 0.70\ W^2$ and $RMSE_P = 39.2 \pm 15.3$ W (mean ± SD; Table 4).

The red bars in Figures 7–9 indicate the formal outcome evaluation interval from 5 to 30 min. In addition to the variables which were already defined above, a variable denoted $\dot{V}O_{2_{smooth}}$ is shown in Figures 7–9: this is a moving average of 25 values of raw $\dot{V}O_2$, and was computed in order to better allow qualitative/visual assessment of the control results. These plots also show the measured HR data in order to demonstrate the phenomenon of a trend in the HR signal as described in Section 1.

The disturbance test with Subject S03 showed that the controller was able to rapidly reject the effects of changes in stepping cadence (Figure 8). It can be seen that, when the cadence is reduced, an initial rise in oxygen uptake is counterbalanced by the controller in the form of a reduction in P_{target}, resulting in rapid recovery of $\dot{V}O_2$ towards $\dot{V}O_{2_{target}}$ with $RMSE_{\dot{V}O_2} = 0.279$ l/min. The disturbance here was smaller than in a former study of HR control (Riedo & Hunt, 2016). In comparison to that study, the smaller reduction in cadence enabled the subject to follow P_{target} more accurately, resulting in the relatively low value of $RMSE_P = 45.5$ W. Despite the disturbance, the control signal showed smooth and calm behaviour, which is reflected in the low average control signal power of $P_{\Delta P} = 1.11\ W^2$.

A further test with Subject S05 investigated the behaviour of a non-low-pass controller. This test underlines the importance of low-pass characteristics in the controller and, consequently, in the input sensitivity function (cf. Figure 6). The low-pass and non-low-pass tests with Subject S05 are shown for comparison in Figure 9. The low-pass controller shows better results in all performance outcomes. The values for the low-pass vs. non-low-pass controllers were: $RMSE_{\dot{V}O_2} = 0.148$ vs. 0.152 l/min, $P_{\Delta P} = 1.66$ vs. 106.63 W^2 and $RMSE_P = 24.6$ vs. 29.3 W. The most striking difference here is the average control signal power $P_{\Delta P}$, which was two orders of magnitude higher with the non-low-pass controller, reflecting this controller's sensitivity to high-frequency measurement noise and disturbances.

4. Discussion

The aim of this work was to identify and compare oxygen uptake and heart rate dynamics, and to develop and test an oxygen uptake controller for an end-effector gait rehabilitation robot using the stair climbing mode of operation. As stated in Section 1, $\dot{V}O_2$ offers a more direct way to characterize the physiological level of exercise intensity. While the main challenge in feedback control of HR was physiological heart rate variability (Riedo & Hunt, 2016), in the present study the substantial breath-by-breath noise on $\dot{V}O_2$ was of primary concern.

The identification of $\dot{V}O_2$ and HR dynamics was successful for all subjects except for Subject S02 due to excessive noise causing fluctuation of the $\dot{V}O_2$ signal. In a previous study, Schindelholz and Hunt (2015), Subject S05 completed a $\dot{V}O_2$ identification using an exoskeleton-type rehabilitation robot (Lokomat, Hocoma AG, Switzerland). The findings there of $k = 0.0238$ (l/min)/W and $\tau = 48.3$ s are very close to the values obtained here on the G-EO with $k = 0.0227$ (l/min)/W and $\tau = 47.1$ s. A comparison of the mean $\dot{V}O_2$ time constant here of $\tau = 53.4$ s (Table 2) with the mean time constant of six subjects running normally on a treadmill found in Hunt, Ajayi, Gollee, & Jamieson (2008) of $\tau = 47.1$ s, indicates that $\dot{V}O_2$ dynamics are similar across very different exercise modalities. Furthermore, the time constant for oxygen uptake dynamics according to Wasserman, Hansen, Casaburi, & Whipp (1999) is generally on the range $\tau = 40 - 60$ s at medium intensity. The mean HR time constant $\tau = 67.3$ s

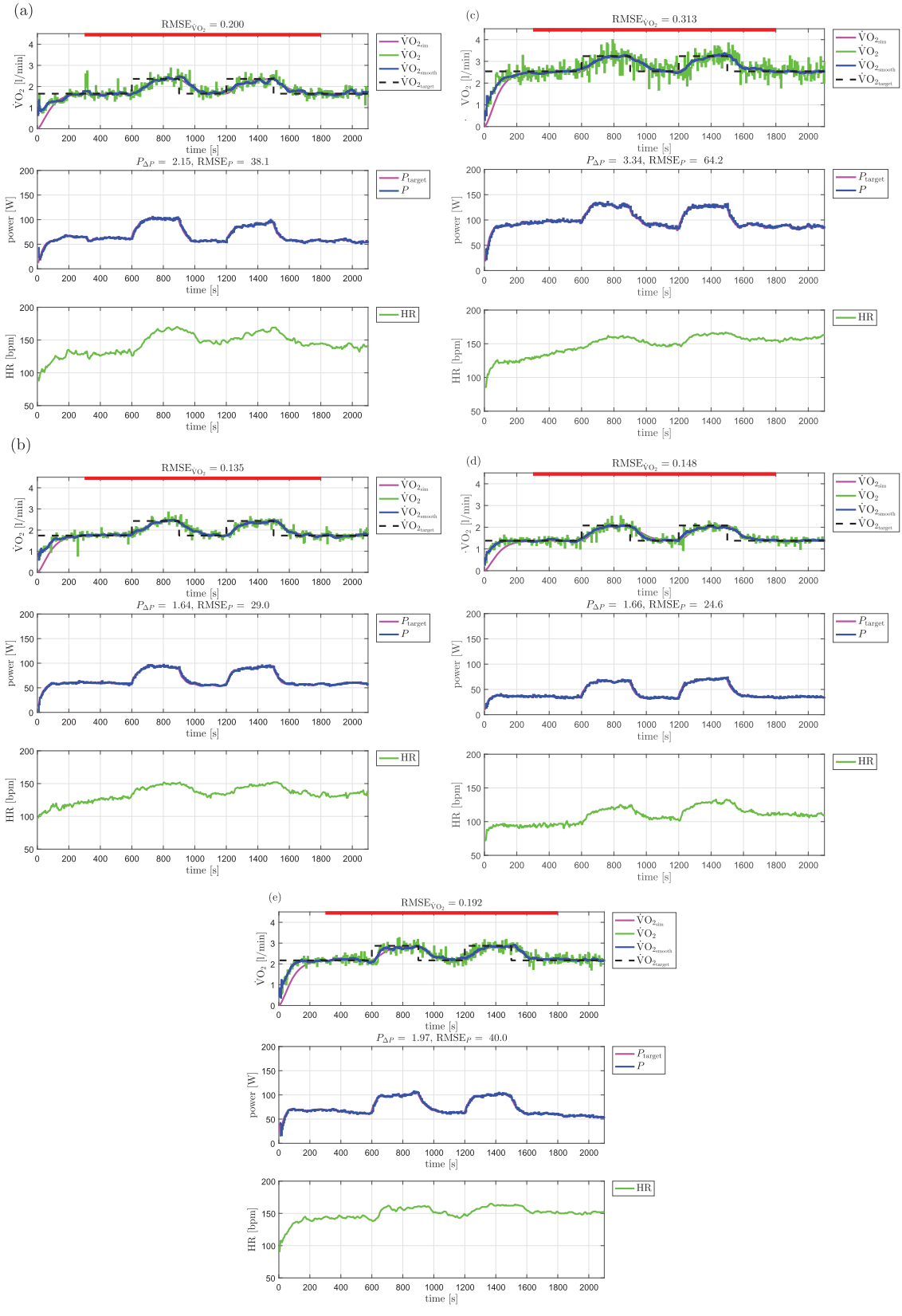

Figure 7. Command response tests. (a) S01, command response test, (b) S03, command response test, (c) S04, command response test, (d) S05, command response test and (e) S06, command response test.

can be compared with a study (Hunt et al., 2015) conducted with 24 subjects running on a treadmill, which revealed a time constant of 57.6 s. Thus all $\dot{V}O_2$ and HR identification results from the present study are in broad agreement with previous reports using differing exercise devices.

The identification of $\dot{V}O_2$ and HR dynamics using a single test for each subject provided a good basis for direct comparison of the respective time constants. Previous studies suggest that τ for HR is generally higher than for $\dot{V}O_2$ (Bearden & Moffatt, 2001; Zhang et al., 2014). The statistical analysis of the five data sets obtained here confirm this hypothesis for the end-effector robot form of exercise, with a p-value for the observed difference of 0.048.

The command response tests showed highly accurate and fast tracking performance for all subjects evaluated, with low RMSE outcomes. The control signal, which in this application is the target work rate to be achieved by volitional control of the subject, displayed calm and smooth behaviour throughout, with a low value of average control signal power. This property is important because it eases the subject's volitional control task.

Robustness was tested by using a controller which was specific to only one subject, i.e. the nominal model for controller calculation was taken as the identified model for Subject S06. The results showed good robustness properties because there was no substantial difference in any of the controller performance outcome measures between the identification subject and the others.

The results demonstrate a very strong positive correlation between RMS tracking error and average control signal power. Ranking these variables according to Table 4, it is apparent that $\text{RMSE}_{\dot{V}O_2}$ and $P_{\Delta P}$ have the same order when ranked, i.e. the subject with the highest $\text{RMSE}_{\dot{V}O_2}$ also has the highest $P_{\Delta P}$, and so on. The correlation coefficient for these two variables was computed as $r = 0.9920$ ($p = 0.0009$). This result suggest that, for feedback control of $\dot{V}O_2$, the individual level of breath-by-breath noise is the principal determinant of objective controller perfor-

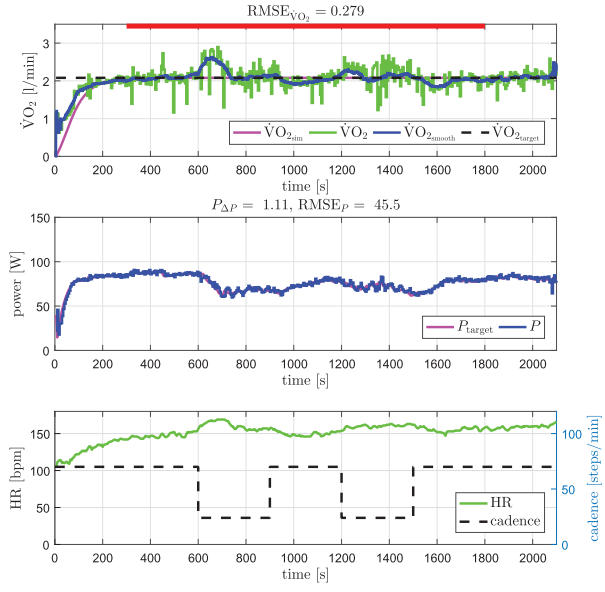

Figure 8. Disturbance rejection test, Subject S03.

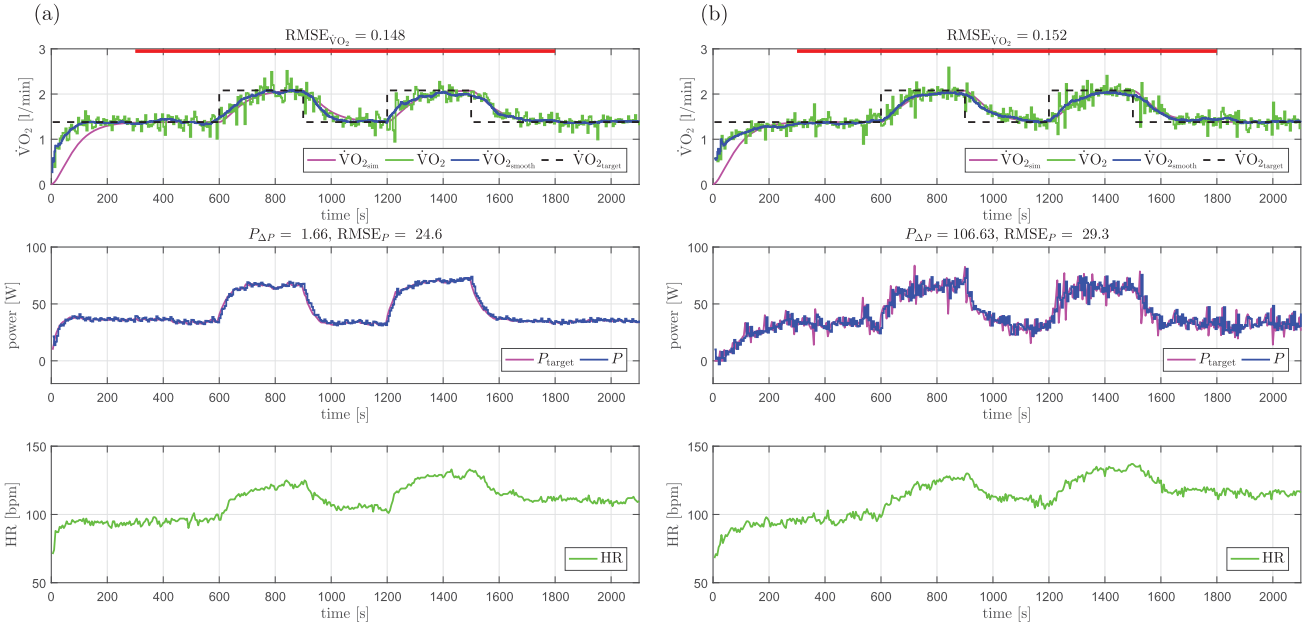

Figure 9. Command response tests of Subject S05 with low-pass controller (left) and with non-low-pass controller (right). (a) Command response with low-pass controller and (b) Command response with non-low-pass controller.

mance, whereas the controller tuning parameter t_r likely plays a secondary role.

The single disturbance test with Subject S03 showed a good disturbance rejection performance. The controller showed good behaviour and was able to bring $\dot{V}O_2$ back to the target in a short time after the perturbation caused when stepping cadence was changed.

The essential difficulty encountered in this work was the substantial breath-by-breath noise observed with some subjects. Moreover, this phenomenon appeared to vary considerably between subjects. This difficulty was overcome by purposely shaping the frequency response of the input sensitivity function to be low pass, such that the control signal remained calm for even worst-case subjects displaying the strongest noise effects.

The importance of this design strategy can be seen in the single test with a non-low-pass controller, which clearly illustrates the importance of suppression of high-frequency noise and disturbances in this application. With the non-low-pass controller, the average control signal power $P_{\Delta P}$ was very high, which substantially increased the cognitive load on the subject and made it very difficult for him to follow the rapidly changing control signal P_{target}. Despite the highly dynamic control signal, where the controller reacted to even small deviations in $\dot{V}O_2$, $\text{RMSE}_{\dot{V}O_2}$ was still higher than for the low-pass controller. Thus, low-pass characteristics of the controller are essential in this case.

A limitation of the present work is that only healthy, able-bodied subjects were included. Further study is required for application to patients who might have cardiopulmonary or cardiovascular disease. Such patients should be subjected to specific identification experiments in case the plant model gains and time constants are substantially different to the ones employed here, which might in turn warrant recalculation of the controller parameters.

A further limitation is that only a small number of subjects was studied, within the limited age range of 23–26 (with the exception of Subject S05, aged 52). Although S05 was not used for determination of the nominal model parameters, he was included in the feedback control experiments; the stable and accurate results achieved with this subject, and with all other subjects, point empirically to an inherent robustness of the feedback system. Nevertheless, future work should include both male and female subjects from target populations of patients undergoing rehabilitation due to neurological deficits, and who will likely be in an older age range than the subjects used in the present work. These investigations should focus first on identification of model parameters and analysis of any differences to the values obtained here.

5. Conclusions

The proposed feedback control strategy for oxygen uptake, $\dot{V}O_2$, was found to be feasible during robotics-assisted stair climbing in healthy subjects. Using quantitative outcome measures, highly accurate and stable control performance was observed in the command response and disturbance rejection tests. Robustness was demonstrated on an empirical basis because a single LTI controller was used which was specific to just one of the subjects, yet the outcome measures were similar across all subjects. The hypothesis that the time constant τ of HR is significantly higher than that for $\dot{V}O_2$ was confirmed. Subject-specific differences in breath-by-breath respiratory noise is the main challenge in the design of feedback control systems for $\dot{V}O_2$. Further clinical testing of this approach with target groups of neurologically impaired subjects is warranted.

Acknowledgements

The authors gratefully acknowledge the contribution made to this work by Matthias Schindelholz (Institute for Rehabilitation and Performance Technology, Bern University of Applied Sciences), who developed the user interface and the Labview structures for the controllers.

Disclosure statement

No potential conflict of interest was reported by the authors.

ORCID

Jan Riedo http://orcid.org/0000-0003-3684-9156
K.J. Hunt http://orcid.org/0000-0002-6521-9455

References

Åström, K. J., & Wittenmark, B. (2011). *Computer controlled systems: Theory and design* (3rd ed.). Mineola, NY: Dover Publications.

Bearden, S. E., & Moffatt, R. J. (2001). $\dot{V}o_2$ and heart rate kinetics in cycling: Transitions from an elevated baseline. *Journal of Applied Physiology*, *90*(6), 2081–2087.

Billinger, S. A., Arena, R., Bernhardt, J., Eng, J. J., Franklin, B. A., Johnson, C. M., … Tang, A. (2014). Physical activity and exercise recommendations for stroke survivors: A statement for healthcare professionals from the American heart association/American stroke association. *Stroke*, *45*(8), 2532–2553.

Chang, W. H., & Kim, Y.-H. (2013). Robot-assisted therapy in stroke rehabilitation. *Journal of Stroke*, *15*(3), 174–181.

Donnan, G. A., Fisher, M., Macleod, M., & Davis, S. M. (2008). Stroke. *The Lancet*, *371*(9624), 1612–1623.

El-Tamawy, M. S., Abd-Allah, F., Ahmed, S. M., Darwish, M. H., & Khalifa, H. A. (2014). Aerobic exercises enhance cognitive functions and brain derived neurotrophic factor in ischemic stroke patients. *NeuroRehabilitation*, *34*(1), 209–213.

French, B., Thomas, L. H., Leathley, M. J., Sutton, C. J., McAdam, J., Forster, A., … McMahon, N. (2007). Repetitive task training

for improving functional ability after stroke. *Cochrane Database System Review*, *17*(4), Cd006073.

Garber, C. E., Blissmer, B., Deschenes, M. R., Franklin, B. A., Lamonte, M. J., Lee, I. M., ... Swain, D. P. (2011). American college of sports medicine position stand, quantity and quality of exercise for developing and maintaining cardiorespiratory, musculoskeletal, and neuromotor fitness in apparently healthy adults: Guidance for prescribing exercise. *Medicine & Science in Sports & Exercise*, *43*(7), 1334–1359.

Hesse, S., Tomelleri, C., Bardeleben, A., Werner, C., & Waldner, A. (2012). Robot-assisted practice of gait and stair climbing in nonambulatory stroke patients. *Journal of Rehabilitation Research and Development*, *49*(4), 613–622.

Hesse, S., Waldner, A., & Tomelleri, C. (2010). Innovative gait robot for the repetitive practice of floor walking and stair climbing up and down in stroke patients. *Journal of Neuro Engineering and Rehabilitation*, *7*, 30.

Hornby, T. G., Straube, D. S., Kinnaird, C. R., Holleran, C. L., Echauz, A. J., Rodriguez, K. S., ... Narducci, E. A. (2011). Importance of specificity, amount, and intensity of locomotor training to improve ambulatory function in patients poststroke. *Topics in Stroke Rehabilitation*, *18*(4), 293–307.

Hunt, K. J., Ajayi, B., Gollee, H., & Jamieson, L. (2008). Feedback control of oxygen uptake during treadmill exercise. *IEEE Transactions on Control Systems Technology*, *16*(4), 624–635.

Hunt, K. J., & Fankhauser, S. E. (2016). Heart rate control during treadmill exercise using input-sensitivity shaping for disturbance rejection of very-low-frequency heart rate variability. *Biomedical Signal Processing and Control*, *30*, 31–42.

Hunt, K. J., Fankhauser, S. E., & Saengsuwan, J. (2015). Identification of heart rate dynamics during moderate-to-vigorous treadmill exercise. *BioMedical Engineering Online*, *14*, 117.

Hunt, K. J., & Hunt, A. J. R. (2016). Feedback control of heart rate during outdoor running: A smartphone implementation. *Biomedical Signal Processing and Control*, *26*, 90–97.

Kelly, J. O., Kilbreath, S. L., Davis, G. M., Zeman, B., & Raymond, J. (2003). Cardiorespiratory fitness and walking ability in subacute stroke patients. *Archives of Physical Medicine and Rehabilitation*, *84*(12), 1780–1785.

Kenney, W. L., Wilmore, J. H., & Costill, D. L. (2015). *Physiology of sport and exercise* (6th ed.). Champaign, IL: Human Kinetics.

Langhorne, P., Coupar, F., & Pollock, A. (2009). Motor recovery after stroke: A systematic review. *The Lancet Neurology*, *8*(8), 741–754.

MacKay-Lyons, M. J., & Makrides, L. (2002). Exercise capacity early after stroke. *Archives of Physical Medicine and Rehabilitation*, *83*(12), 1697–1702.

Mehrholz, J., & Pohl, M. (2012). Electromechanical-assisted gait training after stroke: A systematic review comparing end-effector and exoskeleton devices. *Journal of Rehabilitation Medicine*, *44*(3), 193–199.

Mozaffarian, D., Benjamin, E. J., Go, A. S., Arnett, D. K., Blaha, M. J., Cushman, M., ... Turner, M. B. (2014). Heart disease and stroke statistics-2015 update. *Circulation*, *131*(4), e29–e322.

Pescatello, L. S., Arena, R., Riebe, D., & Thompson, P. D., (Eds.) (2014). *ACSM's guidelines for exercise testing and prescription* (9th ed.). Philadelphia, PA: Lippincott, Williams and Wilkins.

Riedo, J., & Hunt, K. J. (2016). Feedback control of heart rate during robotics-assisted end-effector-based stair climbing. *Systems Science & Control Engineering*, *4*(1), 223–234.

Robergs, R. A., Dwyer, D., & Astorino, T. (2010). Recommendations for improved data processing from expired gas analysis indirect calorimetry. *Sports Medicine*, *40*(2), 95–111.

Schindelholz, M., & Hunt, K. J. (2012). Feedback control of heart rate during robotics-assisted treadmill exercise. *Technology and Health Care*, *20*(3), 179–194.

Schindelholz, M., & Hunt, K. J. (2015). Feedback control of oxygen uptake profiles during robotics-assisted treadmill exercise. *IET Control Theory Applications*, *9*(9), 1433–1443.

Schmidt, R. A., & Lee, T. D. (2011). *Motor control and learning* (5th ed.). Champaign, IL: Human Kinetics.

Stoller, O., Schindelholz, M., Bichsel, L., & Hunt, K. J. (2014). Cardiopulmonary responses to robotic end-effector-based walking and stair climbing. *Medical Engineering & Physics*, *36*(4), 425–431.

Stoller, O., Schindelholz, M., & Hunt, K. J. (2016). Robot-assisted end-effector-based stair climbing for cardiopulmonary exercise testing: Feasibility, reliability and repeatability. *PloS ONE*, *11*(2), e0148932.

Veerbeek, J. M., van Wegen, E., van Peppen, R., van der Wees, P. J., Hendriks, E., Rietberg, M., & Kwakkel, G. (2014). What is the evidence for physical therapy poststroke? A systematic review and meta-analysis. *PLoS ONE*, *9*(2), e87987.

Wasserman, K., Hansen, J. E., Casaburi, R., & Whipp, B. J. (1999). *Principles of exercise testing and interpretation* (3rd ed.). Baltimore, MD: Lippincott, Williams and Wilkins.

Westlake, K. P., & Patten, C. (2009). Pilot study of lokomat versus manual-assisted treadmill training for locomotor recovery post-stroke. *Journal of NeuroEngineering and Rehabilitation*, *6*, 18.

Zhang, Y., Haddad, A., Su, S. W., Celler, B. G., Coutts, A. J., Duffield, R., ... Nguyen, H. T. (2014). An equivalent circuit model for onset and offset exercise response. *BioMedical Engineering OnLine*, *13*, 145.